SUPPLEMENTAL MATERIAL

Coordinated miRNA activity mediates the cellular transition into dormancy during embryonic diapause

Dhanur P. Iyer[1,2,*], Lambert Moyon[3,*], Lars Wittler[1], Chieh-Yu Cheng[1,2], Francisca R. Ringeling[4], Stefan Canzar[4,5], Annalisa Marsico[3,§], Aydan Bulut-Karslioglu[1,§]

Supplemental Figures S1-S10 with legends

Supplemental Fig S1

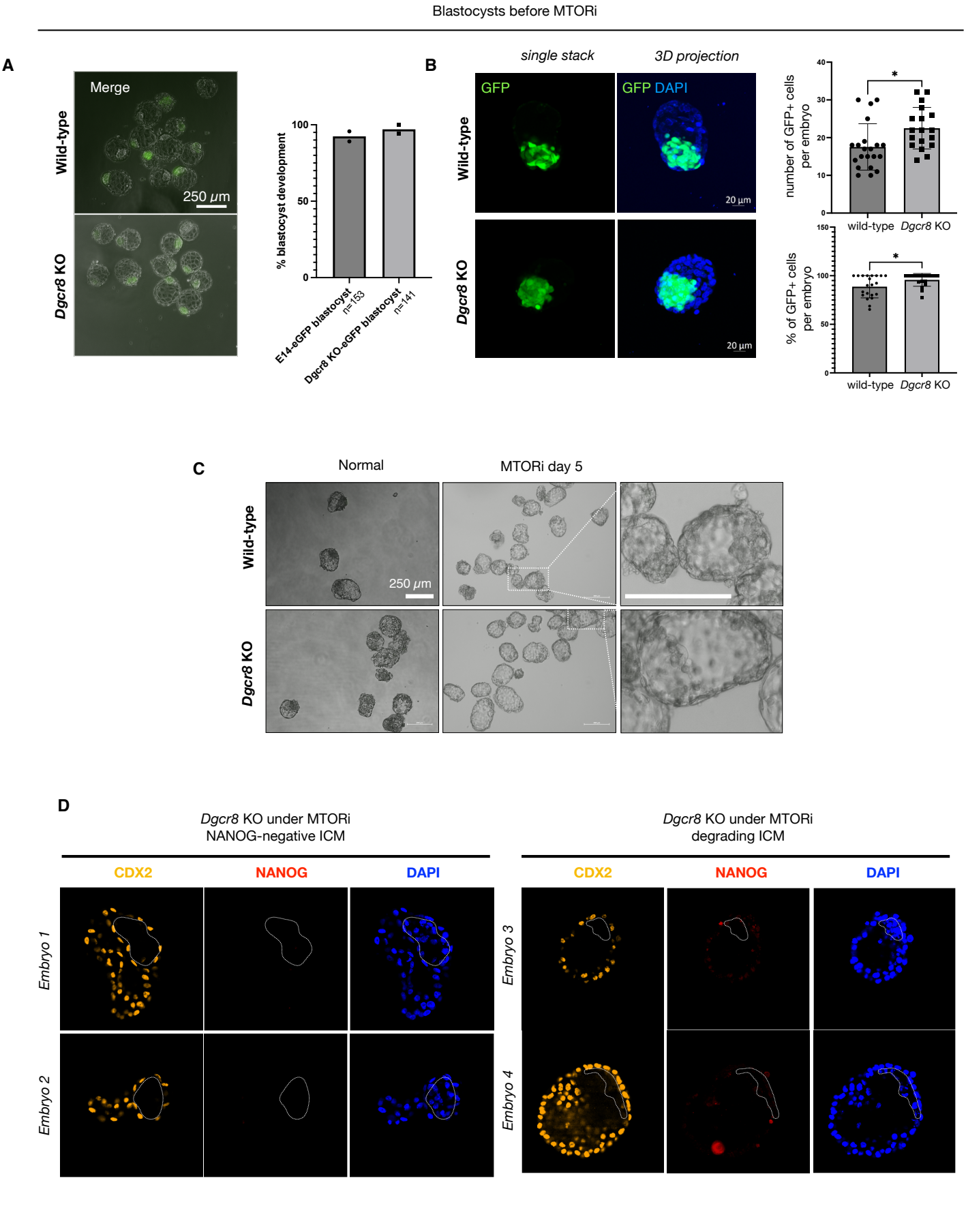

Supplemental Fig S1 Characterisation of chimeric wild-type and *Dgcr8* KO embryos

A. Left, bright field-fluorescence overlays of wild-type and *Dgcr8* KO chimeric embryos. EGFP signals show the ESC contribution to the embryos. Right, blastocyst formation rate (%) of both genetic backgrounds. n, number of embryos. Scale bar, 250 μm.

B. Left, direct fluorescence of embryonic cells in chimeric embryos. Right, quantification of the number and percentage of GFP+ cells in chimeric embryos. Both wild-type and *Dgcr8* KO ESCs contribute to the ICM in chimeric embryos, however, *Dgcr8* KO ESCs contribute a higher percentage. Wild-type chimeric embryos (n=21). *Dgcr8* KO chimeric embryos (n=18).

Scale bar, 20 μm. Statistical test is unpaired *t*-test with Welch's correction.

C. Bright field images of wild-type and *Dgcr8* KO chimeric embryos on day 5 of MTORi treatment. Scale bar, 250 μm.

Right panels show higher magnification images of the area marked with white boxes. A representative *Dgcr8* KO embryo lacking a visibly large ICM is shown.

D. Single z-stack images of *Dgcr8* KO blastocysts under MTORi. CDX2, NANOG, and DAPI stainings are shown. The dashed line marks the ICM or its remnants. The embryos retain blastocoel cavities. Scale bar, 20 μm.

Supplemental Fig S2

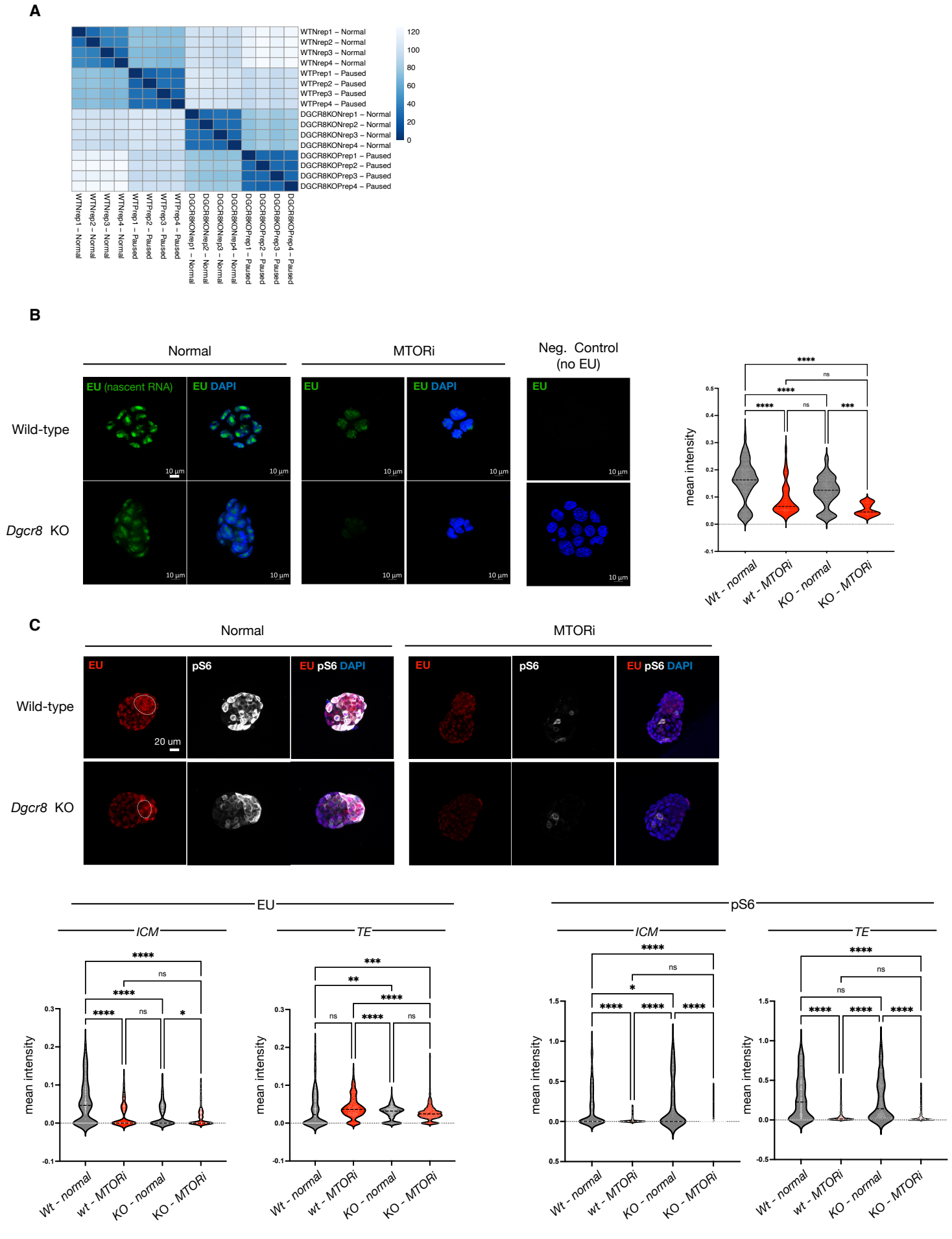

Supplemental Fig S2 Further characterization of wild-type and *Dgcr8* KO ESCs and chimeric embryos

A. Correlation heatmap of bulk RNA-seq datasets of wild-type and *Dgcr8* KO ESC under normal and MTORi conditions. The scale represents the Euclidean distance (calculated on rlog transformed counts) between the samples.

B. Left, analysis of nascent RNA expression levels of wild-type and *Dgcr8* KO ESCs in normal or pausing conditions. Cells were labeled with the nucleotide analog EU while live and visualized after fixing through conjugation of a fluorophore to EU via click chemistry. Negative control sample did not receive EU and was subject to the same procedure during all downstream steps. Scale bar, 10 μm. Right, Mean fluorescence intensity at single-cell resolution. CellProfiler was used to mark nuclei using DAPI as reference, and EU intensity was measured within the marker nuclei. Statistical test is one-way ANOVA with multiple testing correction.

C. EU and phospho-S6 stainings in chimeric embryos. Wild-type and *Dgcr8* KO embryos show similar patterns and levels in pausing conditions, indicating that a diapause response is initiated. 11-13 embryos were used. Scale bar, 10 μm. Statistical test is one-way ANOVA with multiple testing correction.

Supplemental Fig S3

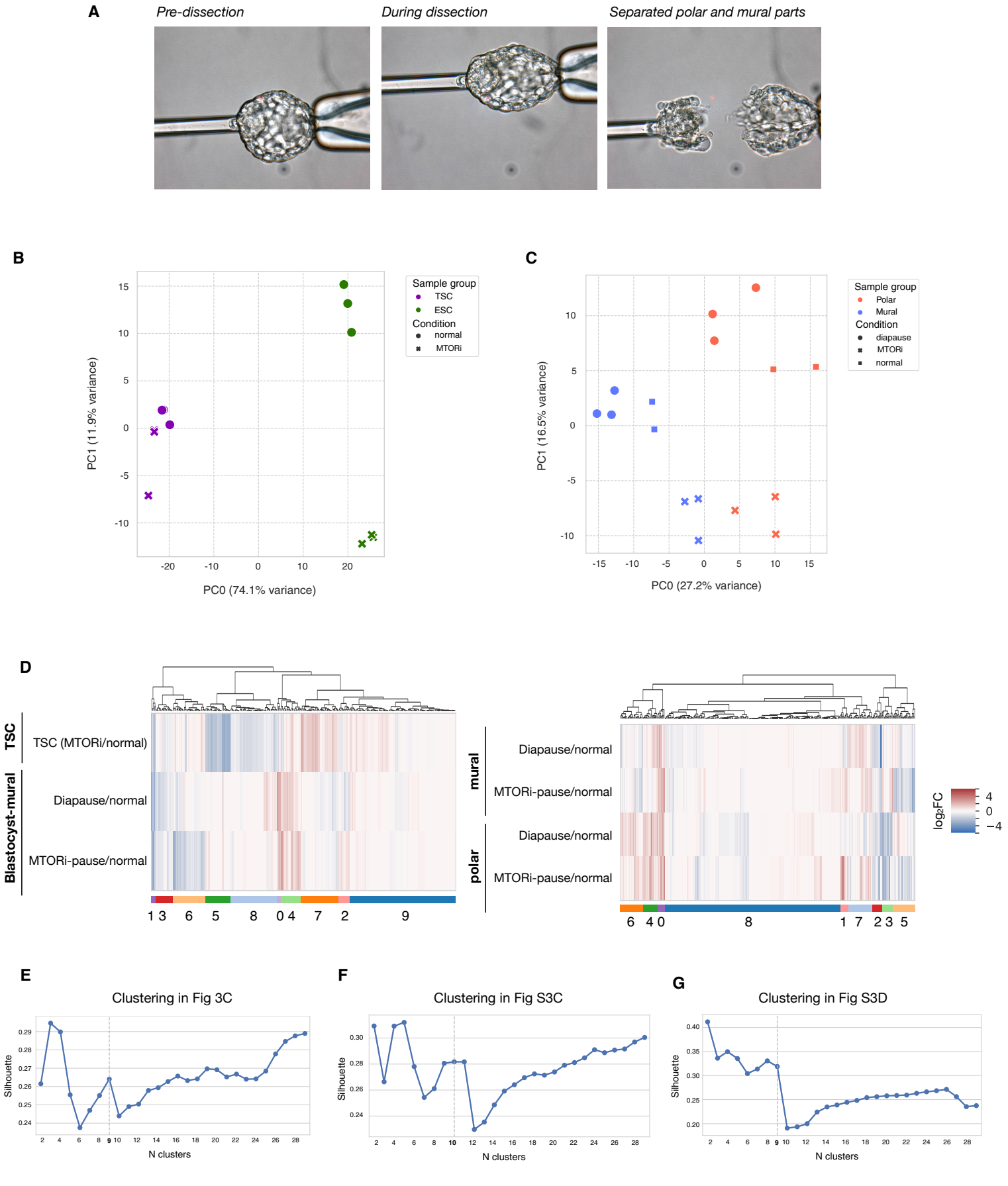

Supplemental Fig S3 Details of miRNA clustering analysis

A. Snapshots taken before, during, and after laser dissection of a representative embryo.

B, C. Separate PCA plots for stem cells (B) and embryos (C), accompanying Figure 3C.

D. Left, heatmap showing miRNA expression changes in the mural side of diapaused embryos (in vitro and in vivo) compared to normal blastocysts, and in paused TSCs compared to normal TSCs. miRNAs were clustered into 10 clusters based on their expression levels in the three samples. Cluster 4 contains concordantly up-regulated miRNAs (N=22), whereas clusters 3 and 1 contain concordantly down-regulated miRNAs (N=18 and 5, respectively). Right, heatmap showing miRNA expression changes in the mural and polar sides of diapaused embryo compared to normal blastocysts. Cluster number 2 contains 10 concordantly up-regulated miRNAs while cluster 2 contains 13 down-regulated miRNAs.

E. Silhouette scores (measuring homogeneity within clusters compared to distance between clusters) for a range of cluster numbers from hierarchical clustering of log_2FoldChange values from MTOR-inhibited ESC, MTOR-inhibited Blastocyst-polar cells, and diapaused Blastocyst-polar cells. The final number of clusters was identified as the best compromise of high-silhouette score and reasonable number of clusters.

F. Silhouette scores for a range of cluster numbers from hierarchical clustering of log_2FC values for TSCs (MTORi/normal) and embryos (in vivo- and in vitro-diapaused blastocyst mural part/normal E3.5).

G. Silhouette scores for a range of cluster numbers from hierarchical clustering of log_2FC values for diapaused embryos compared to normal blastocysts.

Supplemental Fig S4

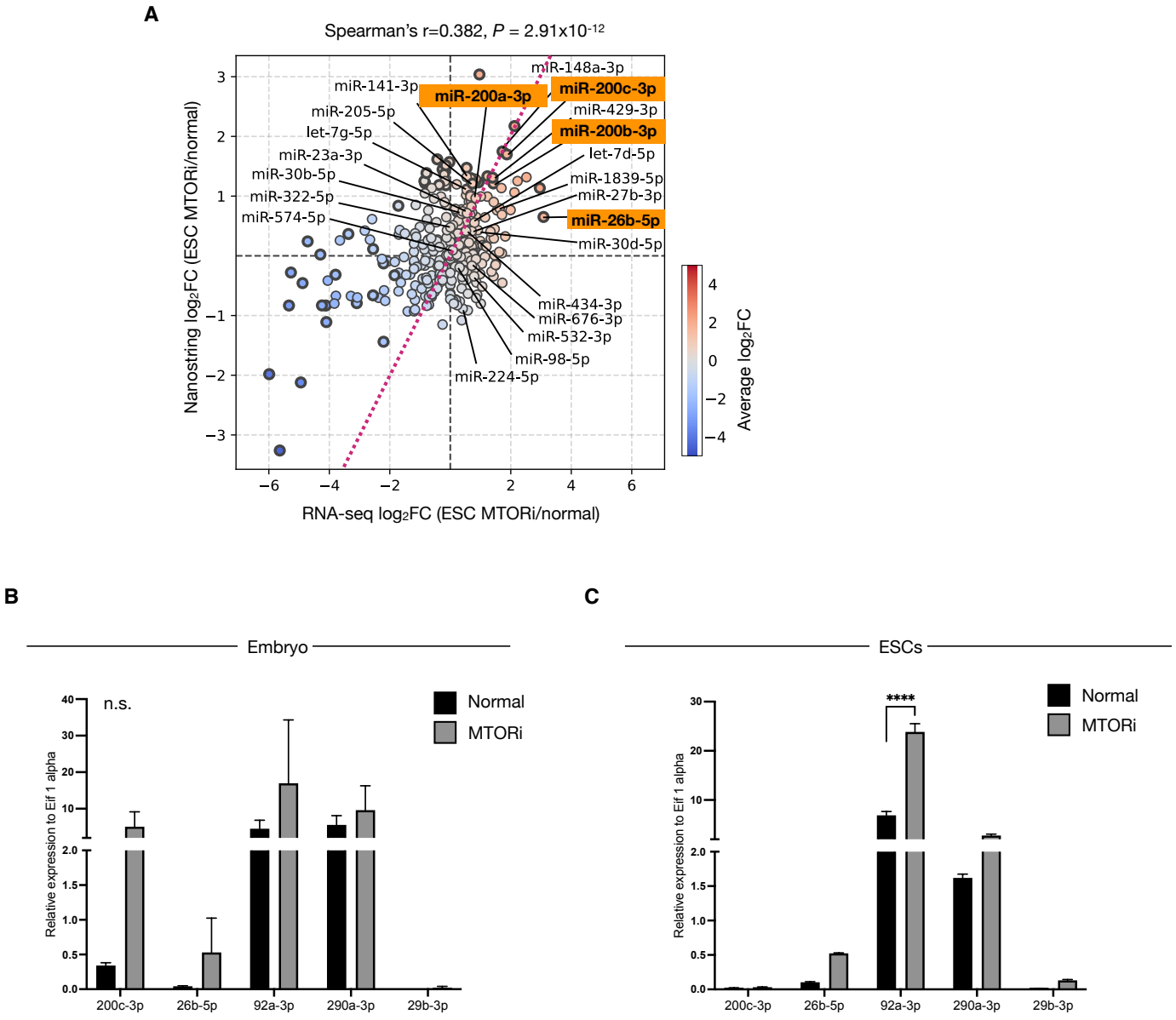

Supplemental Fig S4 Further validation of miRNA expression patterns

A. Comparison of miRNA expression levels resulting from small RNA-seq and Nanostring analyses. Overall, miRNA expression levels correlate, with miR-200 family showing the highest fold changes in both assays.

B. TaqMan qPCR to validate the expression of top enriched miRNAs isolated from normal (n=40) and in vitro-diapaused embryos (n=38). Statistical test is two-way ANOVA with multiple testing correction.

C. TaqMan qPCR to validate the expression of top enriched miRNAs isolated from normal and in vitro-diapaused ESCs. Statistical test is two-way ANOVA with multiple testing correction.

Supplemental Fig S5

A

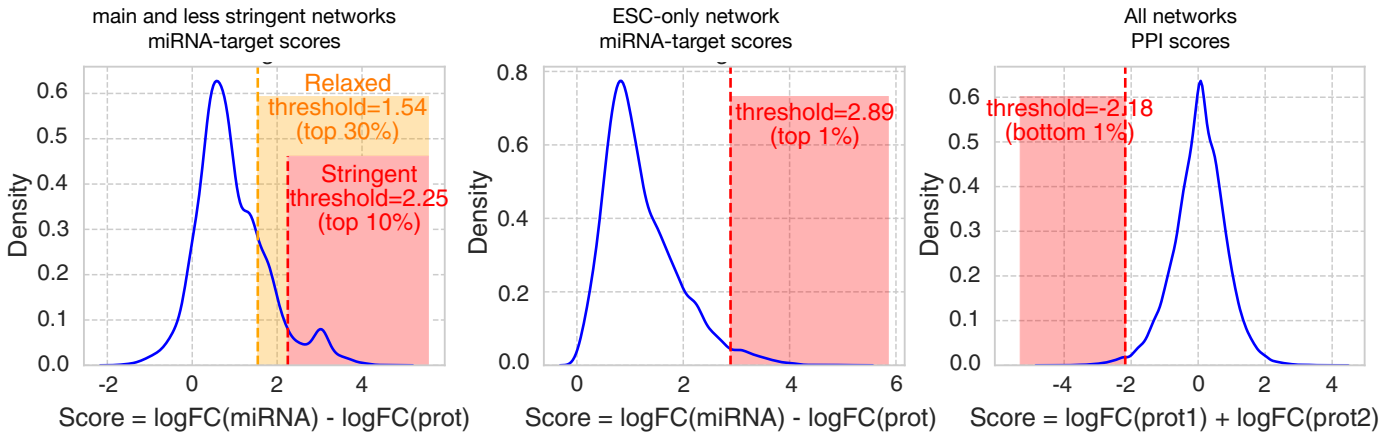

B

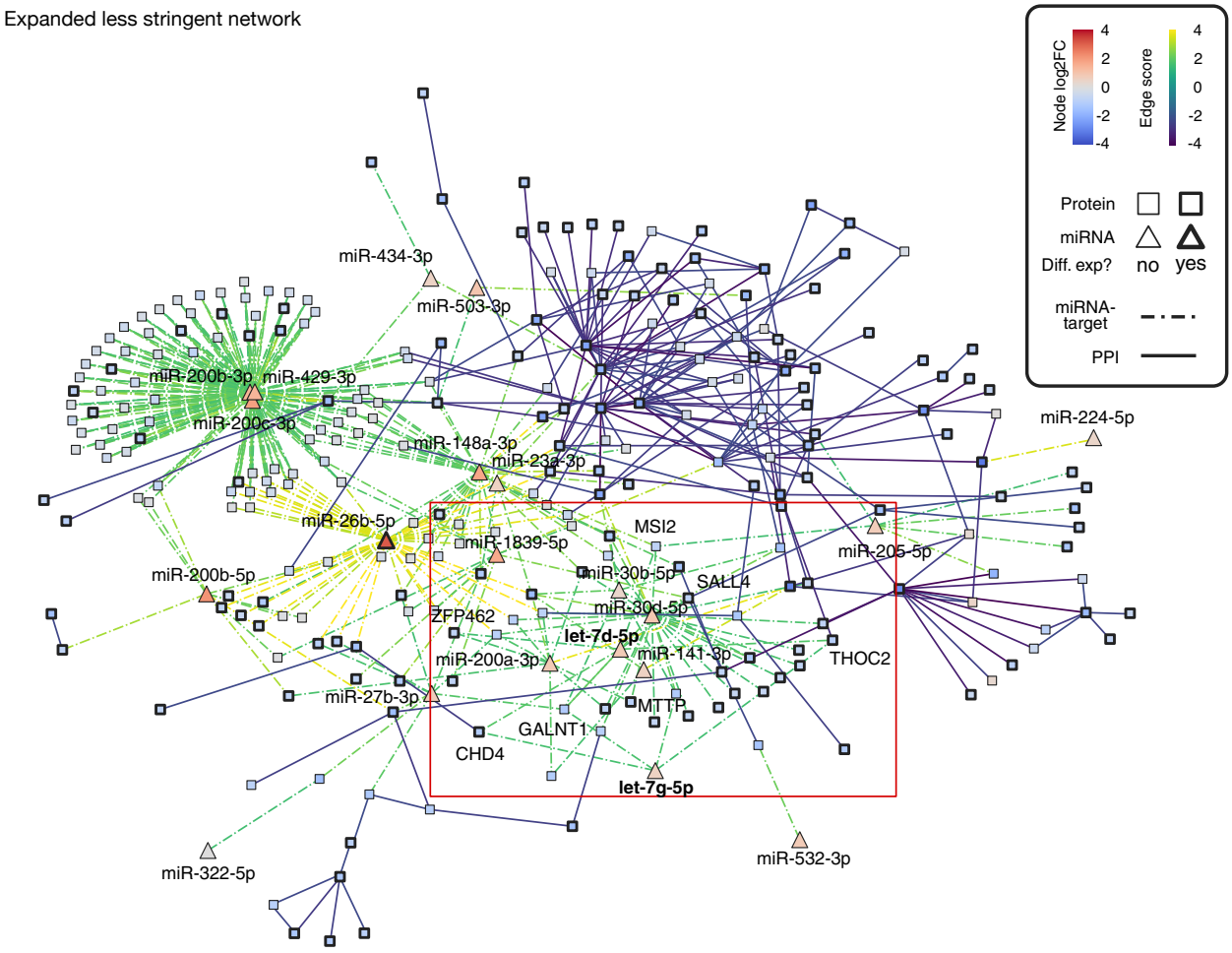

Supplemental Fig S5 A less stringent network includes the let-7 miRNA.

A. Network stringency thresholds. miRNA-target edges were scored as the difference in logFCs between the miRNAs and the target protein, while protein interactions were scored with the sum of logFCs. (Left) A subset of miRNAs was identified from their concordant up-regulated pattern across Blastocyst-polar pausing and ESC pausing, leading to a selection of miRNA-target edges with the visualized distribution of miRNA-target edge scores, from which two high-scoring sets were defined. (Middle) Similarly, a second subset of miRNAs was defined, from their positive logFCs values in MTORi ESC only, and top scoring edges were selected for. (Right) across all networks, protein-protein interactions were filtered for the bottom 1% lowest-scoring, indicative of co-down-regulation.

B. An extended, less stringent miRNA-target network of dormancy. let-7, a previously reported miRNA associated with mouse diapause (Liu et al. 2020), is visible in this network, however it does not pass the stringency threshold in the main network in Fig 4C. A total of 8 target proteins are found, including significantly down-regulated proteins CDH4 (logFC=-1.107, adjusted-P-value=0.0048) and THOC2 (logFC=-1.048, *P*adj=0.017) targeted by both, while SALL4 (logFC=-0.862, *P*adj=0.0172) and ZFP462 (logFC=-0.791, *P*adj=0.011) are additionally targeted by let-7-d.

Supplemental Fig S6

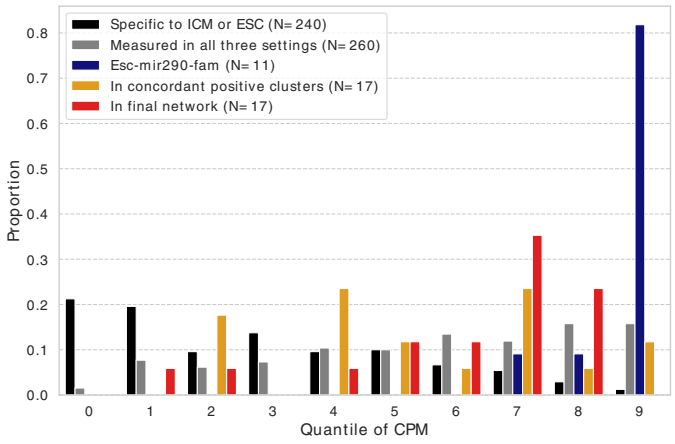

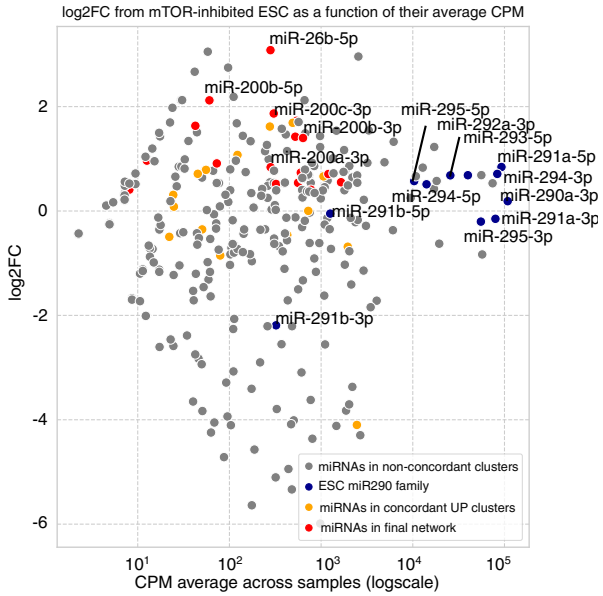

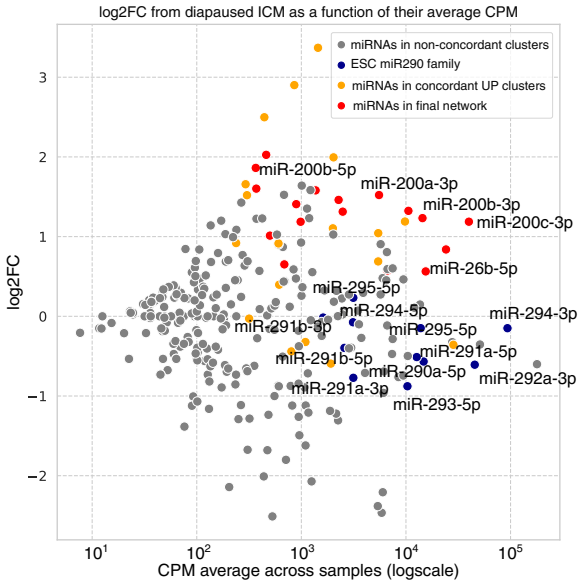

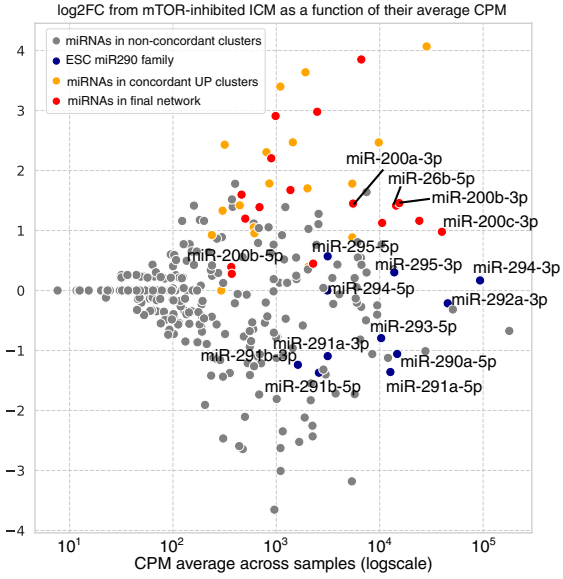

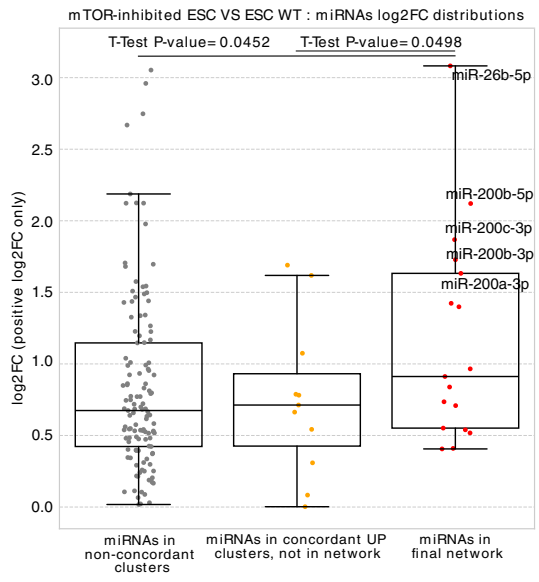

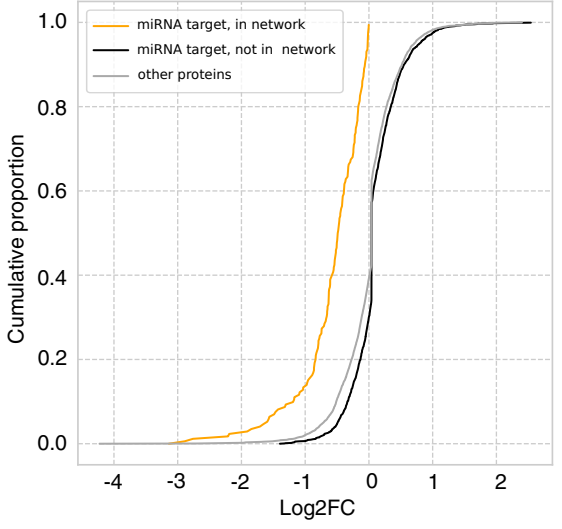

Supplemental Fig S6 Properties of the genes in the regulatory networks

A. Proportions of miRNAs across quantiles of Counts Per Million. We separated miRNAs that are expressed in only in vitro or in vivo samples from miRNAs expressed across all samples, and further separated the candidate miRNAs that were in the clusters of concordant up-regulation from the subset that was retained in the final network. For reference, miRNAs from the miR-290 family, strong markers of ESCs, are also separated in their group.

B-D. Relation between the CPM and the log_2FCs in paused samples compared to normal controls for MTOR-inhibited ESCs (B), diapaused Polar cells (C) and MTOR-inhibited Polar cells (D).

E. (In relation to B) Distributions of the log_2FC patterns of miRNAs after network assignment and filtering.

F. Cumulative distributions of proteomics log_2FC range after network assignment and filtering.

Supplemental Fig S7

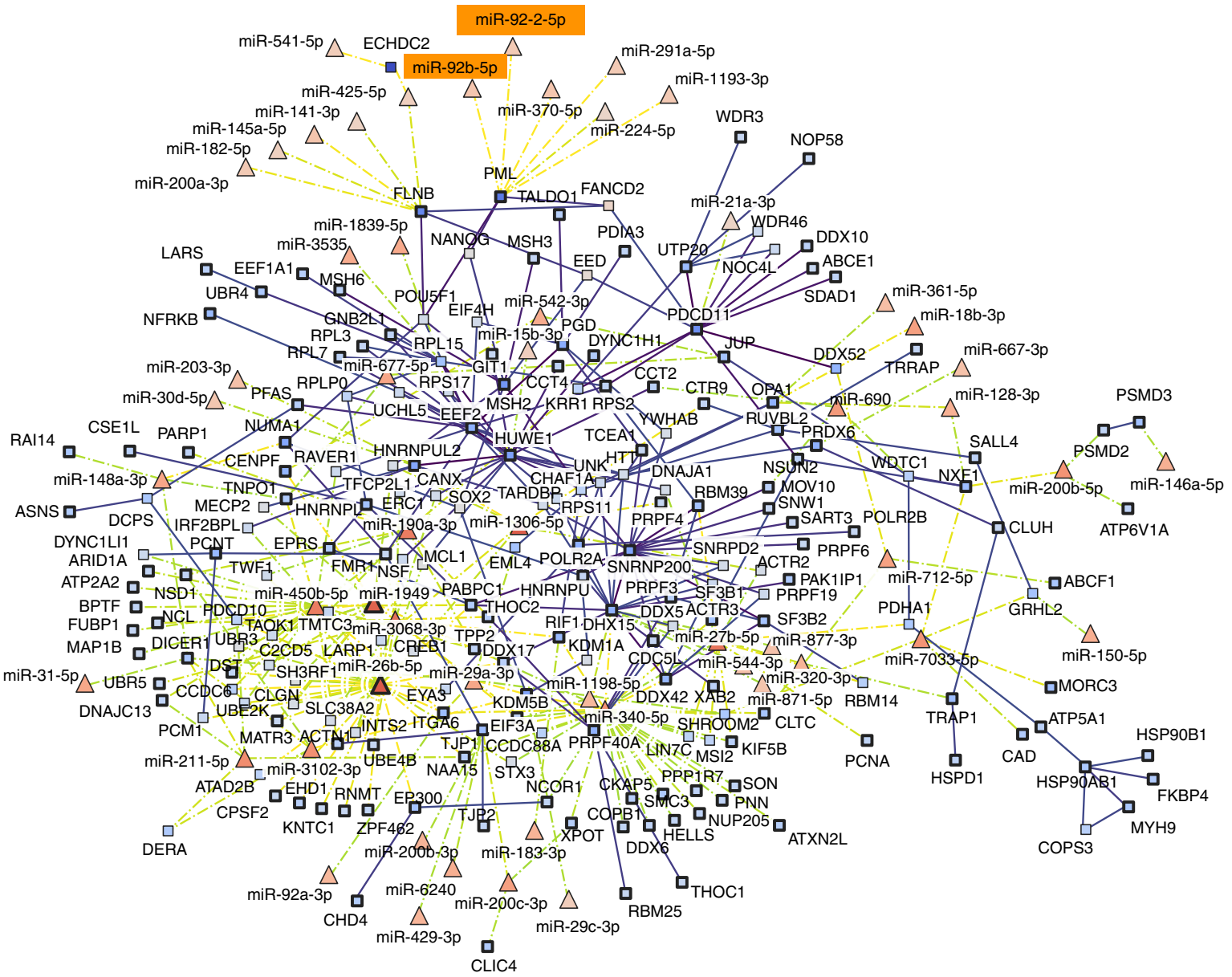

Supplemental Fig S7 The miRNA-target network of ESC pausing

miRNA expression and proteome profiles of MTORi vs normal ESCs were used to construct the ESC-only network. The same stringency cutoff (top 10% of miRNA-target edges, and top 1% of PPIs) as the main network (Fig 4C) was applied. In addition to miR-200 family and miR-26, this network also recovers an evolutionarily conserved regulator of quiescence, miR-92 (Kasuga et al. 2013).

Supplemental Fig S8

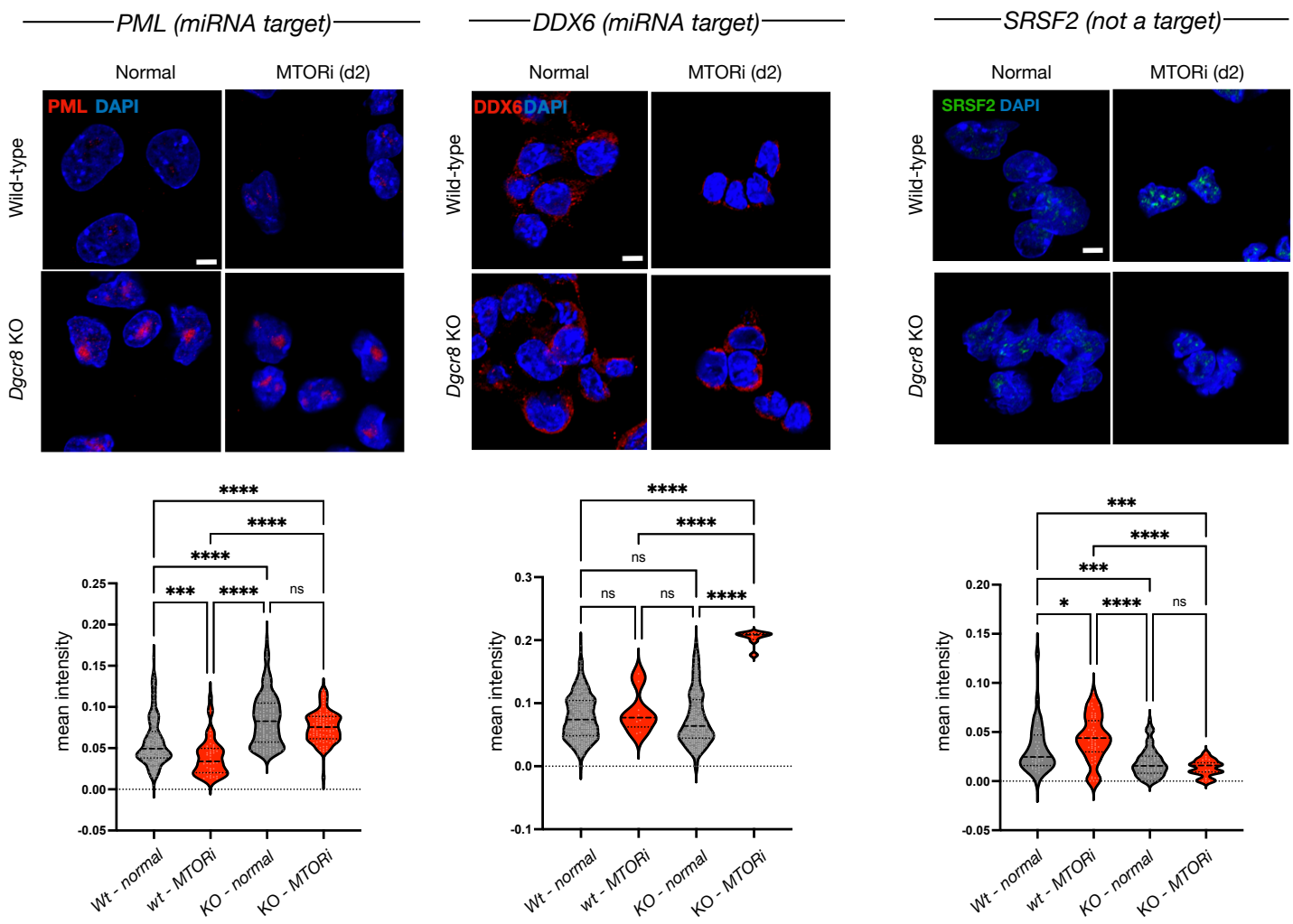

Supplemental Fig S8 The Further characterization of DDX6 and PML expression

IF stainings and single-cell quantifications of PML and DDX6 (in-network) and SC35 (control) proteins in wild-type and *Dgcr8* KO cells in normal and pausing conditions (day 2). Scale bar, 5 μm. Statistical test is one-way ANOVA with multiple testing correction.

Supplemental Fig S9

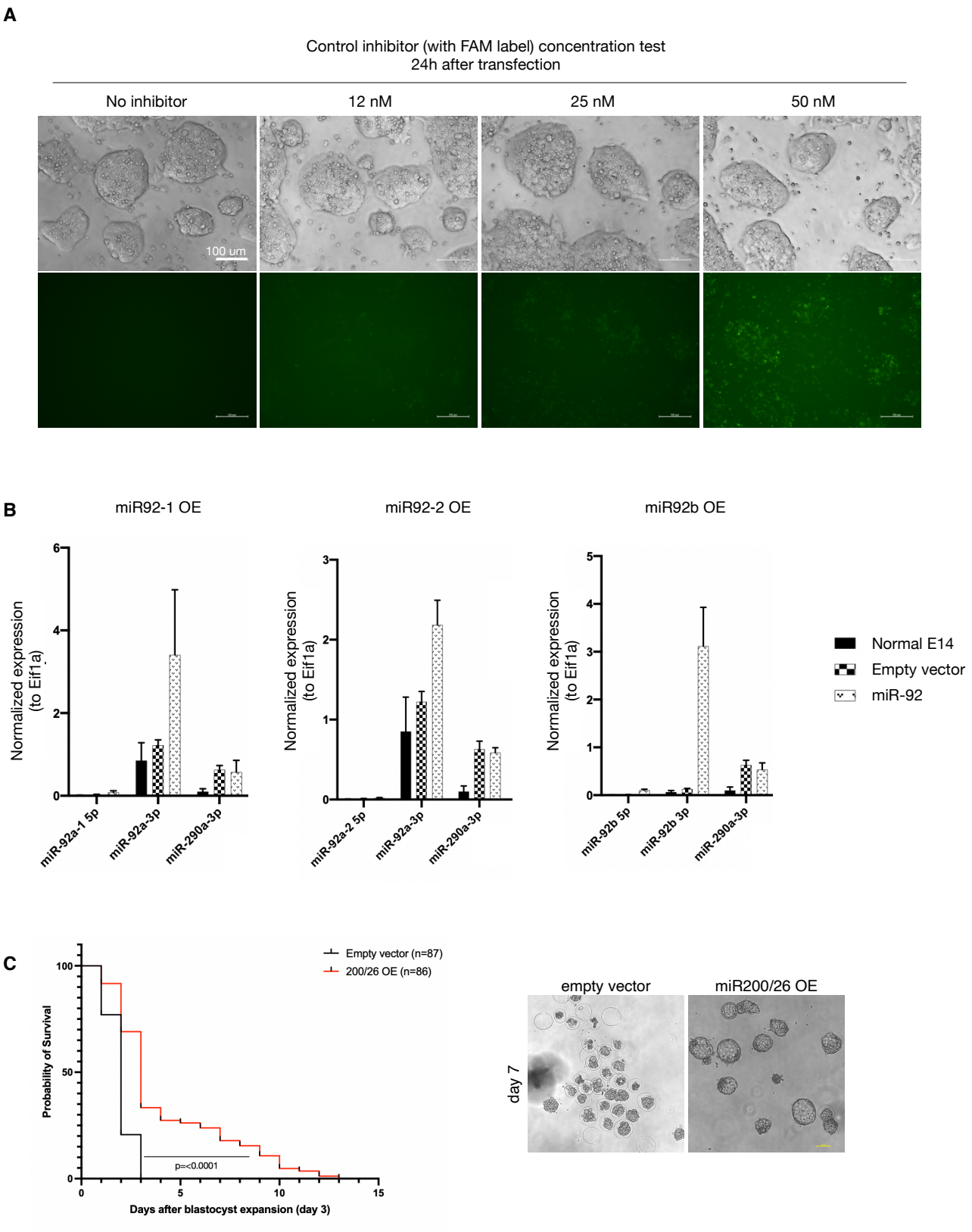

Supplemental Fig S9. Characterization of miRNA inhibition and overexpression

A. Dilution series to determine the appropriate concentration for miRNA inhibitor treatments. FAM-labeled control inhibitor was used to visualize cellular intake. ESCs were transfected with the miRNA and imaged 24h later. 50 nM was chosen as the optimum concentration for use on embryos. Scale bar, 100 μm.

B. qPCR validation of *miR92* overexpression. Wild-type ESCs were transduced with virus carrying *miR92-1/-2/b* or the corresponding empty vector. Expression levels of processed miRNAs (miR-92-1/2-3p or miR-92b-3p) were assessed using specific TaqMan probes. miR-290a-3p was used as control. Of note, miR-92-1- and miR-92-2-3p arms have the same sequence.

C. Survival curves of *miR200/26* OE or control embryos. n, number of embryos in each group. Statistical test is Mantel-Cox test. Right panel shows bright field images of the embryos on day 7. Scale bar, 100 μm.

Supplemental Fig S10

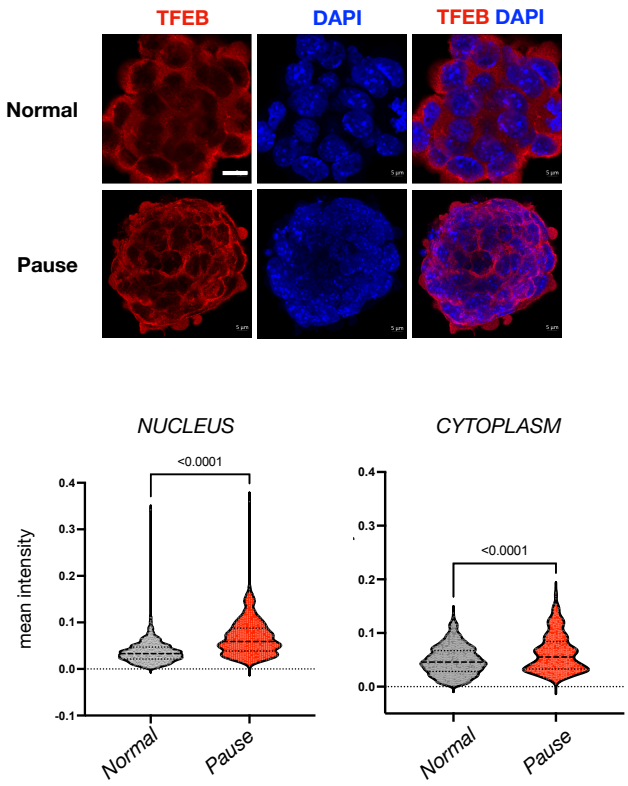

Supplemental Fig S10 TFEB expression and subcellular localization in ESCs

TFEB staining in wild-type normal and paused ESCs. Lower panels show single-cell quantifications of mean fluorescence intensity in the nucleus and cytoplasm. Scale bar, 5 μm. Statistical test is Kolmogorov-Smirnov test, two-sided.